Caffeine adsorption on biochar and subsequent desorption using solvents and supercritical CO2

Biomass and Bioenergy 213 (2026) 109372

Contents lists available at ScienceDirect

Biomass and Bioenergy

journal homepage: www.elsevier.com/locate/biombioe

Caffeine adsorption on biochar and subsequent desorption using solvents and supercritical CO_2

Heejin Lee [a], Silvia Fiore [a,b], Franco Berruti [a,*]

[a] Institute for Chemicals and Fuels from Alternative Resources, Faculty of Engineering, Western University, London, Ontario, Canada
[b] DIATI (Department of Environment, Land, and Infrastructure Engineering), Politecnico di Torino, Corso Duca Degli Abruzzi 24, Torino, 10129, Italy

ARTICLE INFO

Keywords:
Adsorption
Biochar
Caffeine
Desorption
Supercritical CO_2

ABSTRACT

Caffeine is an emerging contaminant frequently detected in aquatic environments, and its effective removal and adsorbent regeneration remain key challenges for sustainable water treatment. In this study, caffeine adsorption and subsequent adsorbent regeneration were investigated using two activated biochars derived from birchwood pellets and miscanthus, with a commercial mineral-derived activated carbon as a reference. Adsorption performance was evaluated through batch experiments by optimizing contact time and pH conditions. The miscanthus-derived activated biochar exhibited the highest caffeine adsorption capacity (up to 176 mg g^{-1}) at optimal pH condition, outperforming both birchwood-derived biochar (97 mg g^{-1}) and commercial activated carbon (172 mg g^{-1}), despite having a lower specific surface area. This behavior was attributed to differences in pore structure and surface functional groups, highlighting the importance of surface chemistry beyond surface area alone. Regeneration of caffeine-loaded adsorbents was examined using solvent desorption with various solutions, as well as supercritical CO_2 ($scCO_2$) extraction. Polar organic solvents, particularly ethanol and methanol, achieved the highest desorption efficiencies, reaching 78% for ASMB, while acidic, alkaline, and aqueous media exhibited markedly lower efficiencies (<27%). Supercritical CO_2 enabled solvent-free regeneration, with desorption efficiencies ranging from 20 to 35% strongly dependent on adsorbent composition and surface polarity. Carbon-rich adsorbents exhibited higher $scCO_2$ compatibility, while oxygen-rich biochars showed reduced desorption. In conclusion, by directly comparing solvent-based desorption and $scCO_2$ extraction within a single framework, this study provides new insights into the regeneration potential of caffeine-loaded biochars and underscores the role of adsorbent properties in selecting sustainable recovery strategies.

1. Introduction

Caffeine, a widely consumed methylxanthine alkaloid found in coffee (*Coffea*) and tea (*Camellia sinensis*), is commonly used in beverages, food, and pharmaceuticals for its stimulant effects [1,2]. Despite its classification as "Generally Recognized as Safe" by the U.S. Food and Drug Administration, caffeine has raised environmental concerns due to its high solubility in water (21.6 g L^{-1}) and persistence in aquatic ecosystems [3]. A considerable portion of ingested caffeine (1–10%) is excreted unmetabolized, entering wastewater streams where conventional treatment methods are often inadequate for its complete removal [3]. As an emerging contaminant, caffeine has drawn attention for its adverse effects on aquatic organisms and its role as a marker for anthropogenic activity [4]. For instance, even concentrations as low as 0.5 μg L^{-1} of caffeine impaired immune function in mussels (*Mytilus galloprovincialis*) after 7 days, while 18 μg L^{-1} caused metabolic disruption and oxidative stress in mollusks like *Ruditapes philippinarum* over 28 days [4]. Due to its widespread presence, the U.S. Environmental Protection Agency identifies caffeine as a wastewater contamination tracer, emphasizing the need for improved removal strategies [4]. While advanced oxidation processes, membrane filtration, and biodegradation have been explored, these methods face challenges such as high cost, limited efficiency, and secondary pollution risks [4,5].

Adsorption-based techniques have emerged as a promising alternative for caffeine removal from water due to their simplicity, cost-effectiveness, and potential for adsorbent regeneration. Biochar, a carbonaceous material produced via the pyrolysis of biomass under limited oxygen, has gained attention as a sustainable and versatile

This article is part of a special issue entitled: Biochar IV published in Biomass and Bioenergy.

* Corresponding author.
E-mail address: fberruti@uwo.ca (F. Berruti).

https://doi.org/10.1016/j.biombioe.2026.109372
Received 28 January 2026; Received in revised form 31 March 2026; Accepted 31 March 2026

adsorbent due to its high surface area, porosity, and functional group diversity, which enhances organic contaminant adsorption [6,7]. Its renewability, low cost, and carbon sequestration potential further support its potential for sustainable water treatment. Recent studies have demonstrated that biochar derived from a variety of biomass sources – including Tingui shells [8] and plant like *Gliricidia sepium* [3] – exhibits substantial caffeine adsorption capacities, with values ranging from 87 mg g^{-1} to 190 mg g^{-1} depending on production conditions and modifications [3,8]. Caffeine adsorption mechanisms were explored, for example, a study on bagasse-derived biochar has shown a direct correlation between apparent surface area, pore structure, and maximum caffeine adsorption capacity, highlighting pore filling as a dominant mechanism for small, planar molecules such as caffeine (molecular radius ≈ 0.376 nm) [9]. In addition to diffusion-controlled pore filling, π–π donor-acceptor interactions between the aromatic structure of caffeine and carbonaceous surfaces, hydrophobic interactions, and hydrogen bonding associated with oxygen-containing functional groups (e.g., phenolic and carbonyl groups) collectively enhance caffeine retention on biochar surfaces [9]. Similarly, a study on engineered egusi seed shell biochars produced at higher pyrolysis temperatures demonstrated enhanced caffeine uptake, attributed to increased specific surface area (up to 688 m^2 g^{-1}) and micropore volume, with Langmuir maximum adsorption capacities of approximately 121 mg g^{-1} [2]. Spectroscopic analyses further indicated that oxygen-containing functional groups (e.g., phenolic and carbonyl groups) facilitate hydrogen bonding with caffeine, while π–π and n–π interactions were also observed under conditions where electrostatic effects are negligible [2]. These structure-property relationships are consistent with adsorption trends reported for aromatic organic contaminants on engineered biochars, where surface area, pore accessibility, and aromaticity were identified as key factors controlling adsorption performance [2,9,10]. More recent studies on advanced carbonaceous adsorbents have similarly highlighted the importance of pore structure, oxygen-containing surface functionalities, and active-site accessibility in governing adsorption performance and interfacial interactions [11–14].

Although adsorption effectively removes contaminants from wastewater, it generates spent adsorbents that pose disposal and regeneration challenges. Consequently, the reusability of spent adsorbents through desorption techniques has become an important focus for improving the sustainability and cost-effectiveness of adsorption processes. Various regeneration approaches, including thermal, ultrasonic, microwave, electrochemical, solvent desorption, and supercritical fluid extraction, have been explored for this purpose [10,15,16]. Among these methods, thermal regeneration of granular activated carbon – the most widely applied industrial approach – typically results in 5–15% carbon loss per regeneration cycle due to burn-off and attrition, along with high energy consumption and CO_2 emission, which substantially increase operational costs and environmental burdens [17,18]. As an alternative, solvent-based desorption efficiencies have been shown to depend strongly on solvent properties, with higher-polarity solvents such as methanol and ethanol exhibiting greater effectiveness through disruption of π–π stacking and hydrogen bonding interactions that retain adsorbates on carbonaceous surfaces [10].

Despite advancements in adsorption research, studies specifically addressing the desorption and regeneration of caffeine-loaded adsorbents remain limited. For example, caffeine-saturated ground coffee waste-derived carbon adsorbents were successfully regenerated through ethanol desorption, enabling multiple adsorption-desorption cycles [19]. Similarly, the reusability of magnetically engineered activated carbon, maintaining approximately 95% caffeine removal efficiency over four cycles, was demonstrated using alkaline solvent regeneration (0.1 M NaOH and water) assisted by ultrasonication [5].

Beyond solvent-based approaches, supercritical fluid extraction offers distinct advantages, including reduced solvent consumption, minimal environmental impact, and enhanced penetration into the porous structure of adsorbents. In particular, supercritical carbon dioxide ($scCO_2$) is appealing due to its moderate critical temperature (31 °C), non-toxicity, non-flammability, and ease of separation from desorbed products [10,20,21]. Despite its limited affinity for polar compounds, $scCO_2$ has demonstrated promising compatibility with caffeine, supporting its potential as a desorption agent. For instance, a 66% caffeine removal efficiency was achieved during $scCO_2$ extraction from Korean green tea at 323 K and 40 MPa [22]. More recent research focusing on the decaffeination of green coffee beans utilized a pressure swing $scCO_2$ extraction method, which successfully achieved nearly 100% decaffeination at 353 K and 30 MPa [23].

Considering the existing literature, several knowledge gaps remain regarding the integrated removal of caffeine and the regeneration of caffeine-loaded carbonaceous adsorbents. To the best of our knowledge, systematic comparisons of biochars with distinct physicochemical properties produced under comparable conditions are scarce while numerous studies have reported caffeine adsorption on individual biochars derived from different feedstocks, limiting the understanding of how feedstock origin and surface chemistry influence caffeine adsorption performance. Moreover, while solvent desorption and $scCO_2$ extraction have been independently investigated for caffeine removal or decaffeination in food systems, a direct comparison of solvent-based desorption and $scCO_2$ extraction for the regeneration of caffeine-loaded adsorbents has not yet been reported. Consequently, the relative effectiveness, selectivity, and regeneration potential of these recovery strategies remain insufficiently understood.

The novelty and main objective of this study lie in the systematic evaluation of both adsorption and recovery stages within a single framework, combining a comparative assessment of biochars with different properties and a direct comparison of solvent and $scCO_2$ desorption for adsorbent recovery. Specifically, this study explores a two-phase process involving caffeine removal from water via adsorption onto biochar, followed by recovery of adsorbent. In detail, the caffeine adsorption performance of two biochars derived from the pyrolysis of birchwood pellets and miscanthus were compared by optimizing key process parameters, including contact time and pH, using a mineral-derived commercial activated carbon as a reference. Birchwood was selected as a representative woody biomass, whereas miscanthus was selected as a herbaceous biomass, allowing comparison of biochars derived from feedstocks with different lignocellulosic composition and mineral content. Subsequently, adsorbent recovery was investigated through solvent extraction using various media (water, ethanol, methanol, 0.1 M sulfuric acid and 0.1 M sodium hydroxide), as well as through supercritical CO_2 extraction.

2. Materials and methods

2.1. Materials and characterization

This study involved two biochars derived from waste biomass feedstocks. Birchwood pellets, obtained from Northern Flame (St. Catharines, Ontario, Canada), were converted into biochar (birchwood pellet biochar, BPB) using a pilot-scale pyrolysis horizontal reactor (PYROH) (Fig. 1) at the Institute for Chemicals and Fuels from Alternative Resources (ICFAR), Western University, Canada. The PYROH reactor operated at a pressure below 5 psi and within a temperature range of 450–500 °C, at a feed rate of 0.3 kg min^{-1}. Standard Miscanthus Biochar (SMB) was purchased from the UK Biochar Research Centre, University of Edinburgh, UK (www.biochar.ac.uk), and was produced via pyrolysis at 450 °C.

Both biochars were physically activated at ICFAR using a 1.3 m-long horizontal fixed-bed tube furnace (Across International, New Jersey, USA) at 900 °C (heating rate of 10 °C·min^{-1}) for 3 h under a constant CO_2 flow of 2 L min^{-1}. These activation conditions were selected based on previous optimization studies reported in our earlier work, in which different CO_2 activation parameters were evaluated and the selected condition provided enhanced adsorption performance of the resulting

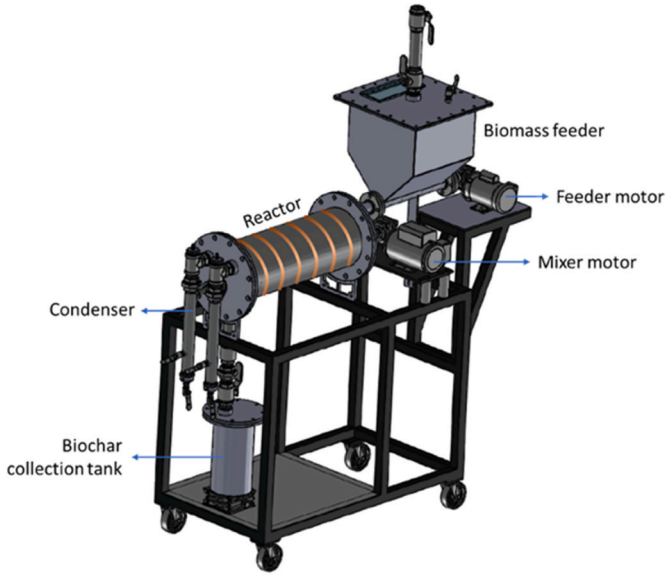

Fig. 1. Outline of the Pyrolysis Horizontal Reactor (PYROH) used to produce the birchwood pellet biochar.

biochar-based adsorbents [10]. CO_2 activation was selected as a physical activation method due to its ability to effectively develop microporosity and increase surface area while avoiding the use of chemical activating agents that may generate secondary waste streams and introduce residual chemicals into the adsorbent structure [24]. The resulting activated biochars are hereafter referred to as ABPB and ASMB. The adsorbents were used in their original pellet form without additional grinding or sieving prior to the adsorption experiments. A commercial mineral-derived activated carbon ($CAC_{minerals}$) supplied by Amtra, Italy (https://amtra.net/en/) was included in all experiments as a reference material.

The physicochemical properties of ABPB, ASMB, and $CAC_{minerals}$ were characterized in triplicate. Brunauer-Emmett-Teller (BET) analysis was performed using liquid nitrogen at −196 °C to determine the specific surface area (SSA) and pore size distribution, employing a Nova 2000e surface area and pore size analyzer (Quantachrome Instruments, Anton Paar Quanta Tec Inc., Florida, USA). Ash content was determined by proximate analysis following the ASTM D1762-84. Surface functional groups were identified using Fourier-Transform Infrared (FTIR) spectrometer (PerkinElmer, Massachusetts, USA). To evaluate the aromaticity, hydrophilicity, and polarity of the adsorbents, H/C, O/C, and (O + N)/C atomic ratios were determined via CHNS elemental analysis using an EA 1112 Series CHNS elemental analyzer (Thermo Fisher Scientific, Massachusetts, USA). The chemical composition was determined by inductively coupled plasma optical emission spectroscopy (ICP-OES) performed by PPB Analytical Inc. (Toronto, Ontario, Canada). The zeta potential of each adsorbent was measured using a Zetasizer Nano ZSP (Malvern Panalytical, Worcestershire, UK).

Caffeine, methanol, and ethanol were obtained from Sigma-Aldrich (Massachusetts, USA). Sulfuric acid was obtained from Caledon (Ontario, Canada) and sodium hydroxide was obtained from Fisher Scientific (Ontario, Canada). All chemical reagents used were of analytical grade. Deionized (DI) water was used in all experimental procedures requiring water.

2.2. Adsorption tests

Batch adsorption tests were carried out using caffeine (500 mg L^{-1}) and the adsorbents ABPB, ASMB and $CAC_{minerals}$ in triplicate. The tests were performed by placing 50 mL of aqueous caffeine solution in contact with the adsorbent at a concentration of 1.0 g L^{-1} at room temperature (298 K) under magnetic stirring. This dosage was selected as a representative condition for the present study based on our previous study [6]. After mixing, the supernatants were collected and filtered through 0.22 μm membrane filters (Maple Lab Systems, Mississauga, Canada). The caffeine concentration in the supernatants was analyzed using a UV-Vis spectrometer at a wavelength of 273 nm [25]. The effect of contact time on adsorption was evaluated by withdrawing and analyzing supernatant samples at fixed times. To investigate the influence of pH on adsorption, the solution pH was adjusted to 2, 7, and 11 using 0.1 M sulfuric acid and 0.1 M sodium hydroxide solutions.

The adsorption capacity (q_e, mg·g^{-1}) and removal percentage were calculated using equations (1) and (2), respectively:

$$\text{Adsorption capacity } \left(\text{mg}\cdot\text{g}^{-1}\right) = q_e = \frac{(C_0 - C_e)\times V}{M} \quad (1)$$

$$\text{Percentage removal } (\%) = \frac{(C_0 - C_e)}{C_0}\times 100 \quad (2)$$

where q_e is the equilibrium uptake capacity of the adsorbent (mg·g^{-1}), C_0 is the initial caffeine concentration (mg·L^{-1}), C_e is the equilibrium caffeine concentration (mg·L^{-1}), V is the solution volume (L), and M is the mass of the adsorbent (g).

2.3. Desorption tests

2.3.1. Solvent desorption

The desorption efficiency of various solvents (methanol, ethanol, 0.1 M H_2SO_4, 0.1 M NaOH, and deionized (DI) water) towards caffeine was examined by placing 100 mg of spent adsorbent from the adsorption tests in contact with 100 mL of solvent under magnetic stirring for 20 h, a contact time selected based on previous adsorption-desorption studies reporting that extended desorption periods are often required depending on the adsorbate-adsorbent binding strength [26,27]. Previous studies have similarly employed desorption contact times of several hours for the solvent regeneration of carbonaceous adsorbents [28–30]. Then, the concentration of desorbed caffeine in the solvent was analyzed using UV-Vis spectroscopy at 272 nm with a UV-Vis Onda UV30 Scan spectrometer. The amount of substance desorbed was calculated using equation (3), while the desorption efficiency was determined as a percentage using equation (4):

$$\text{Desorbed amount } \left(\text{mg}\cdot\text{g}^{-1}\right) = q_d = \frac{C_d\times V}{W} \quad (3)$$

$$\text{Desorption efficiency } (\%) = \frac{q_d}{q_a}\times 100\% \quad (4)$$

where q_d (mg·g^{-1}) is the desorbed amount,

C_d (mg·L^{-1}) is the concentration of the desorbed substance in the solvent, V (L) is the volume of the solvent, W (g) is the weight of the adsorbent, and q_a (mg·g^{-1}) is the total amount of sorbate initially adsorbed on the adsorbent.

2.3.2. Supercritical CO_2 desorption

Supercritical CO_2 desorption experiments were conducted using a bench-scale supercritical fluid extractor unit (Fig. 2), which was specifically designed and assembled for this study. The unit was constructed of 316 stainless steel and included an extraction chamber (outer diameter 60.3 mm, inner diameter 42.8 mm, total volume 0.3 L) equipped with a band heater (Zesta, Mississauga, Ontario, Canada), a 2000-psi pressure gauge, and a fast-acting pressure relief valve. Two collection chambers, each equipped with a 600-psi pressure gauge, were placed in a water bath (ice packs were added during cooling to lower the temperature to approximately 15 °C). To control and safely release pressure, a back-pressure regulator was installed between the collection chambers and the vent leading to the fume hood. To prevent clogging from oil or solid particles, an oil filter was positioned before the back-pressure

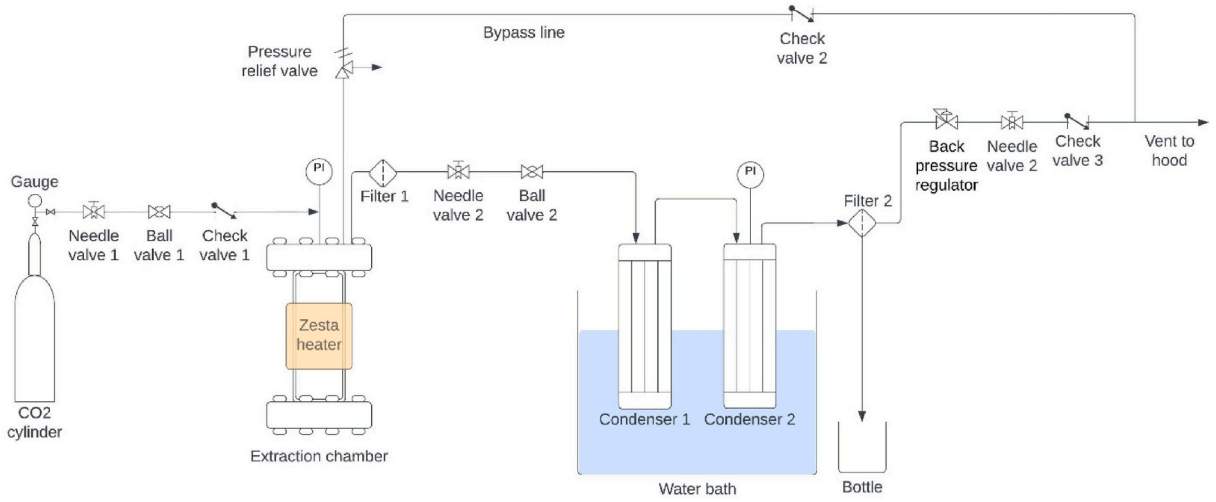

Fig. 2. Outline of the supercritical CO_2 extraction system.

regulator. The system included three needle valves, located before the extraction chamber, between the extraction and collection chambers, and between the collection chambers and the vent. A bypass line was incorporated to directly connect the extraction chamber to the back-pressure regulator, providing a safety mechanism in case of pipeline failure between the extraction and collection chambers.

During the supercritical CO_2 desorption tests, the extraction chamber was filled to its full volume with each adsorbent, which had been pre-loaded with caffeine under adsorption conditions to achieve saturation, then securely sealed and liquid CO_2 was introduced. The temperature was then raised to 60 °C, resulting in pressures exceeding 1150 psi, and the extraction was carried out for 1 h. Subsequently, the caffeine-CO_2 mixture was transferred to the collection chambers for an additional 1 h to ensure separation of caffeine from CO_2. To achieve complete desorption, the entire procedure was repeated under the same conditions. The system was tested with commercial GAC saturated with caffeine and then operated with samples of spent adsorbent derived from the batch adsorption tests. The amount of desorbed caffeine ($W_{desorbed}$) was calculated using equation (5), while the desorption efficiency (E_d) was calculated from the weight difference of the spent adsorbent before ($W_{initial}$) and after (W_{final}) the double-extraction using equation (6):

$$W_{desorbed}(g) = W_{initial}(g) - W_{final}(g) \quad (5)$$

$$E_d(\%) = \frac{W_{desorbed}}{W_{adsorbed}} \times 100\% \quad (6)$$

where $W_{initial}$ (g) is the weight of the spent adsorbent before desorption,
W_{final} (g) is the weight of the adsorbent after desorption,
$W_{desorbed}$ (g) is the weight of the caffeine desorbed,
$W_{adsorbed}$ (g) is the initial amount of adsorbed caffeine, and.
E_d (%) is the desorption efficiency.

3. Results and discussion

3.1. Characterization of adsorbents

The elemental composition and ash content of the feedstock, biochars, and activated adsorbents are presented in Table 1. The birchwood pellet feedstock (BPF) exhibited moderate carbon content and low ash content. After pyrolysis, the resulting birchwood pellet biochar (BPB) showed a substantial increase in carbon content and a decrease in H/C and O/C ratio, reflecting the progressive carbonization and devolatilization that occur during thermal conversion [31]. For the miscanthus-derived material, the standard miscanthus biochar (SMB) exhibited a higher ash content compared to BPB, which is consistent with the generally higher mineral content of herbaceous biomass.

A high ash content can restrict the formation of micropores during the development of mesopores, thereby limiting the increase in specific surface area (SSA) and total porosity [32]. The formation of mesopores is often associated with the catalytic effect of inorganic compounds in ash, which facilitates the conversion of micropores into mesopores [33]. ASMB exhibited the highest ash content but had the lowest SSA and micropore surface area compared to ABPB and $CAC_{minerals}$. The elevated ash content in ASMB is likely attributed to inorganic mineralization and the presence of impurities in the feedstock during pyrolysis [34]. Ash,

Table 1
Elemental composition and ash content of feedstock, biochars, and activated adsorbents (BPF: birchwood pellet feedstock; BPB: birchwood pellet biochar; ABPB: activated birchwood pellet biochar; SMB: standard miscanthus biochar; ASMB: activated standard miscanthus biochar; $CAC_{minerals}$: commercial activated carbon derived from minerals).

Adsorbents		BPF	BPB	ABPB	SMB	ASMB	$CAC_{minerals}$
Ash content [%]		0.57	2.72	14.25	12.15	34.34	13.51
Elemental analysis	C [%]	46.28	89.61	76.62	75.41	41.68	79.16
	H [%]	6.80	1.26	0.05	2.42	0.19	0.00
	N [%]	0.58	0.00	0.00	0.78	0.00	3.91
	S [%]	0.00	0.00	0.00	-	0.00	0.00
	O[b] [%]	45.76	6.40	9.08	9.24	23.79	3.42
Atomic ratio	H/C	1.75	0.17	0.01	0.38	0.06	0.00
	O/C	0.74	0.05	0.09	0.09	0.43	0.03
	(O + N)/C	0.75	0.05	0.09	-	0.43	0.07

[a]The analyses are obtained from the UK biochar research center.
[b]The oxygen content was calculated by the difference and subtracted the ash content.

particularly inorganic components such as alkali and alkaline earth metals, may enhance adsorption performance through mechanisms such as ion exchange and electrostatic interactions [35].

The H/C, O/C, and (O + N)/C atomic ratios serve as key indicators of the structural and chemical characteristics of the adsorbents, including aromaticity, hydrophilicity, and polarity, respectively [31]. A lower H/C ratio signifies a greater degree of carbonization and higher aromaticity, while an increase in the O/C atomic ratio suggests enhanced hydrophilicity. Similarly, a high (O + N)/C ratio corresponds to greater polarity. ABPB exhibited a lower H/C ratio than ASMB, indicating a higher degree of carbonization and greater aromaticity. In contrast, ASMB displayed higher O/C and (O + N)/C ratios compared to ABPB and $CAC_{minerals}$, suggesting that ASMB has greater hydrophilicity and polarity. These findings highlight the distinct physicochemical properties of each adsorbent, which significantly influence their adsorption behavior and potential applications in pollutant removal from aqueous systems.

The FTIR spectra of ABPB, ASMB, and $CAC_{minerals}$ (Fig. 3) revealed several characteristic peaks corresponding to key functional groups associated with surface chemistry. The spectral region between 2600 cm^{-1} and 3000 cm^{-1} corresponds to -OH stretching vibrations, characteristic of carboxylic acid functional groups [36]. Peaks observed between 1700 cm^{-1} and 1900 cm^{-1} represent the stretching vibration of the carbonyl (C=O) functional group [36,37]. Additionally, peaks found in the 1300 cm^{-1} to 1600 cm^{-1} range correspond to C=C-C stretching within aromatic rings, signifying the presence of conjugated π-electron systems [36–38]. The presence of C-O stretching vibrations is evident from a distinct peak at 1030 cm^{-1} [36–38], while a peak at 400 cm^{-1} corresponds to aromatic C-H bond stretching [14]. The FTIR findings are consistent with the elemental analysis of the adsorbents. ASMB exhibited the most intense C-O stretching peak, indicating a higher oxygen content relative to the other adsorbents. In contrast, ABPB displayed a stronger peak in the aromatic C=C-C stretching region, suggesting a greater degree of aromaticity and carbonization compared to ASMB. These results highlight the chemical composition differences among the adsorbents, which play a crucial role in their adsorption capabilities and interaction mechanisms with target contaminants.

Table 2 illustrates the substantial increase in SSA of BPB and SMB after activation, from 5.3 $m^2 g^{-1}$ to 437.3 $m^2 g^{-1}$, while that of SMB rose from 33.6 $m^2 g^{-1}$ to 398.3 $m^2 g^{-1}$. Expanded SSA and the creation of porous structures typically increase the number of accessible active sites, which improves the adsorption capacity [39]. $CAC_{minerals}$ had the highest SSA (585.0 $m^2 g^{-1}$), compared to ABPB and ASMB. The differences observed in BET surface area and pore structure may also be associated with the intrinsic properties of the precursor biomass. In particular, the higher ash content observed in the miscanthus-derived material may influence pore development during activation, as mineral components can catalyze structural transformations and affect the formation of micro- and mesopores [32,33]. However, ASMB exhibited the highest exterior surface area (S_{ext}) value at 107.6 $m^2 g^{-1}$, followed by ABPB at 74.9 $m^2 g^{-1}$, and $CAC_{minerals}$ at 71.0 $m^2 g^{-1}$. The nitrogen adsorption-desorption isotherms of ABPB, ASMB, and $CAC_{minerals}$ show Type I behavior, as classified by IUPAC classification [40] (Fig. 4). Type I isotherms, characteristic of microporous materials, display a steep nitrogen uptake at low relative pressures ($P/P_0 < 0.1$), followed by a plateau at higher pressures. This trend indicates the dominance of micropores (diameter <2 nm), where rapid pore filling occurs due to strong adsorbate-adsorbent interactions. The available pore volume appears to be mostly inside the microporous range, according to this adsorption pattern, which restricts further multilayer adsorption at higher pressures [41]. Additionally, the existence of H4 hysteresis loops at the relative pressure surpasses 0.4 indicates a minor contribution of slit-like mesopores (diameter 2–50 nm) to the overall pore structure. These findings highlight the importance of surface area and pore structure for adsorbents, as a well-developed microporous network is crucial for achieving high adsorption efficiency.

The chemical composition of the adsorbents varied significantly (Table 3). Fe was the most abundant element in ABPB (41 g/kg), followed by Ca (25 g/kg) and Ni (12 g/kg). $CAC_{minerals}$ contained the highest level of Ca (5 g/kg), followed by Al (1 g/kg), while Fe and Ni were present at much lower concentrations (452 ppm and 55 ppm, respectively). Al was also notable in ABPB (619 ppm). In ASMB, P was the most abundant element (437 ppm), followed by Ca (327 ppm), whereas Fe, Ni, and Al were detected at much lower concentrations of 69 ppm, 19 ppm, and 6 ppm, respectively. The significantly higher Al content in $CAC_{minerals}$ and ABPB compared to ASMB suggests its potential contribution to structural properties [42]. P was another key element, with 6 g/kg in ABPB compared to 667 ppm in $CAC_{minerals}$. S levels in $CAC_{minerals}$ (170 ppm) and ASMB (19 ppm) were significantly lower than in ABPB (413 ppm).

The point of zero charge (pH_{pzc}) is a crucial factor in determining the surface charge properties of adsorbents. When the aqueous phase pH is

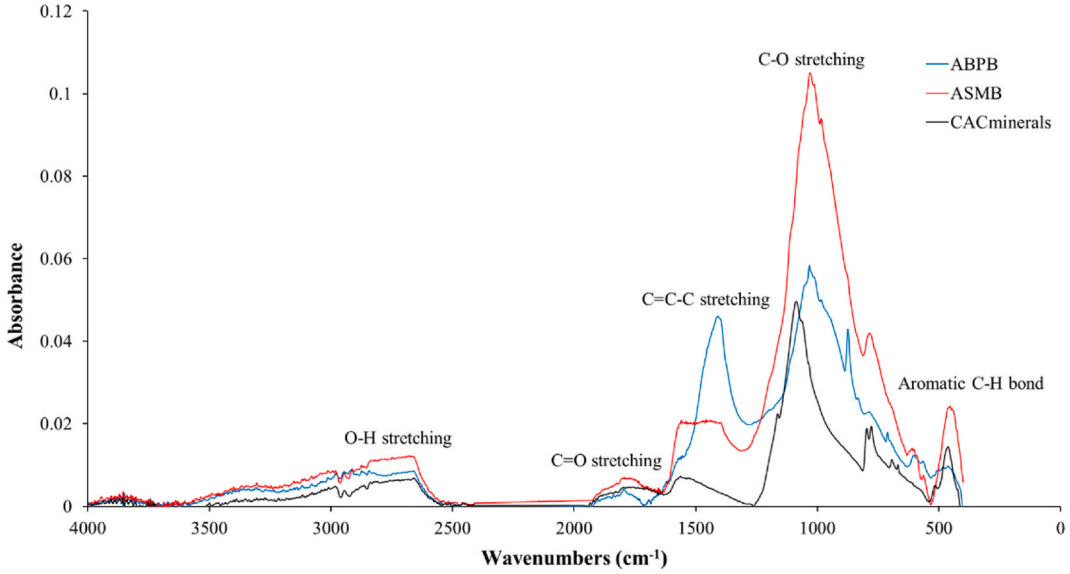

Fig. 3. Fourier-Transform Infrared Spectroscopy (FTIR) of adsorbents (ABPB: activated birchwood pellet biochar; ASMB: activated standard miscanthus biochar; $CAC_{minerals}$: commercial activated carbon derived from minerals).

Table 2
Results of B.E.T. analysis of adsorbents (BPB: birchwood pellet biochar; ABPB: activated birchwood pellet biochar; SMB: standard miscanthus biochar; ASMB: activated standard miscanthus biochar; $CAC_{minerals}$: commercial activated carbon derived from minerals; SSA: specific surface area; S_{micro}: surface area of micropores; S_{ext}: external surface area; V_{total}: total pore volume; V_{micro}: pore volume of micropores).

Adsorbents	SSA ($m^2 \cdot g^{-1}$)	S_{micro} ($m^2 \cdot g^{-1}$)	S_{ext} ($m^2 \cdot g^{-1}$)	V_{total} ($cm^3 \cdot g^{-1}$)	V_{micro} ($cm^3 \cdot g^{-1}$)	Average pore diameter (nm)
BPB	5.3	-	-	-	-	-
ABPB	437.3	362.5	74.9	0.27	0.19	1.24
SMB[a]	33.6	-	-	-	-	-
ASMB	398.3	290.6	107.6	0.27	0.15	1.37
$CAC_{minerals}$	585.0	514.0	71.0	0.33	0.26	1.13

[a] The analysis was obtained from the UK biochar research center.

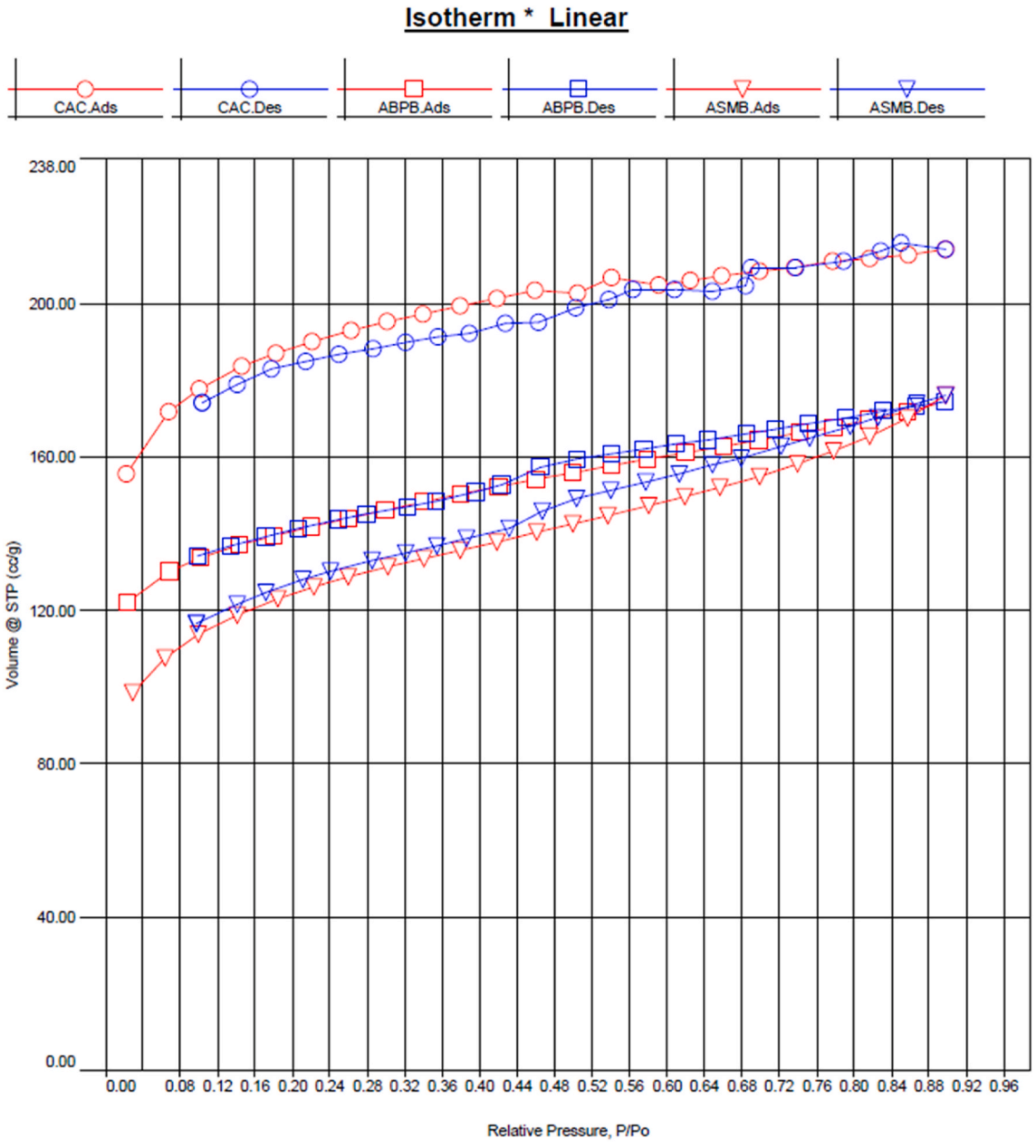

Fig. 4. Nitrogen adsorption-desorption isotherms of the adsorbents (*$CAC_{minerals}$*: commercial activated carbon derived from minerals; ABPB: activated birchwood pellet biochar; ASMB: activated standard miscanthus biochar; Ads: adsorption; Des: desorption.)

below the pH_{pzc}, the adsorbent surface becomes protonated, leading to a positive charge. In contrast, when the pH surpasses the pH_{pzc}, the surface undergoes deprotonation, acquiring a negative charge [39,43]. A positively charged surface promotes the adsorption of anionic pollutants, while a negatively charged surface enhances the adsorption of cationic species due to electrostatic attraction [44]. The pH_{pzc} values measured for the tested adsorbents were determined as 5.3 for ABPB, 3.4 for ASMB, and 5.6 for $CAC_{minerals}$ (Fig. 5). The knowledge of these values

Table 3
Chemical composition of the adsorbents (ABPB: activated birchwood pellet biochar; ASMB: activated standard miscanthus biochar; $CAC_{minerals}$: commercial activated carbon derived from minerals; LOD: limit of detection; LOQ: limit of quantification.)

Chemical element	LOD (ppm)	LOQ (ppm)	ABPB	ASMB	$CAC_{minerals}$
Aluminum	0.010	0.031	618.945	5.798	1006.245
Antimony	0.025	0.074	ND	<LOQ	ND
Arsenic	0.015	0.044	ND	0.678	ND
Barium	0.005	0.015	309.814	2.143	72.262
Beryllium	0.002	0.007	ND	0.085	<LOQ
Cadmium	0.027	0.082	ND	ND	ND
Calcium	0.039	0.117	25004.250	326.652	4828.175
Chromium	0.005	0.014	232.643	0.962	<LOQ
Copper	0.037	0.110	37.260	0.503	ND
Iron	0.011	0.033	40916.125	68.508	451.844
Lead	0.015	0.045	ND	ND	ND
Manganese	0.005	0.014	3980.963	4.168	19.635
Molybdenum	0.007	0.020	452.762	0.613	14.674
Nickel	0.090	0.269	11904.213	18.505	54.606
Phosphorous	0.043	0.128	5839.175	437.130	667.310
Selenium	0.017	0.051	ND	ND	ND
Sulfur	0.009	0.029	412.903	19.284	170.065
Tin	0.017	0.051	103.684	<LOQ	ND
Vanadium	0.034	0.101	<LOQ	<LOQ	<LOQ
Zinc	0.026	0.079	ND	1.954	ND

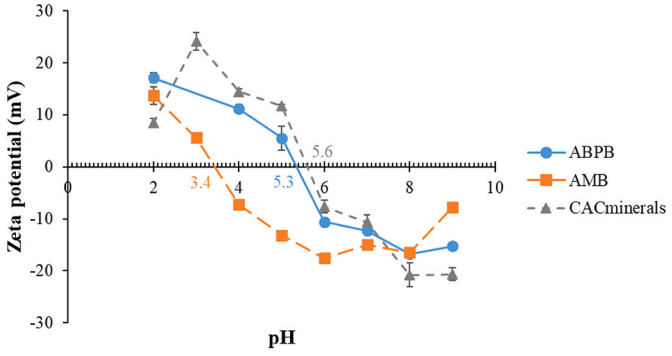

Fig. 5. Values of point of zero charge of the adsorbents (ABPB: activated birchwood pellet biochar; ASMB: activated standard miscanthus biochar; $CAC_{minerals}$: commercial activated carbon derived from minerals; Error bars represent the standard deviation (n = 3)).

is strategic, as by understanding the electrostatic interactions between adsorbents and target pollutants at different pH levels, the solution pH can be adjusted to optimize adsorption efficiency. The lower pHpzc observed for ASMB compared to ABPB can be attributed to the higher abundance of oxygen-containing functional groups on the ASMB surface [45]. These acidic functional groups increase surface acidity and shift the pH_{pzc} toward lower values. This interpretation is consistent with FTIR spectra (Fig. 3), where ASMB exhibits a stronger C-O stretching band, indicating a greater presence of oxygenated surface groups. In contrast, the lower O/C and H/C ratios of ABPB indicate a higher degree of carbonization and aromaticity, which is typically associated with fewer acidic surface groups and therefore a higher pH_{pzc}.

3.2. Adsorption

The optimal contact time was calibrated on the commercial adsorbent. For $CAC_{minerals}$ the recorded adsorption capacities were 38.9 mg g^{-1} at 2 h, 61.0 mg g^{-1} at 3 h, 99.1 mg g^{-1} at 5 h, 129.4 mg g^{-1} at 18 h, 135.9 mg g^{-1} at 20 h, and 136.6 mg g^{-1} at 24 h (Fig. 6). Therefore, 20 h was identified as optimal duration for adsorption experiments.

The results of the adsorption tests (Fig. 7) revealed notable

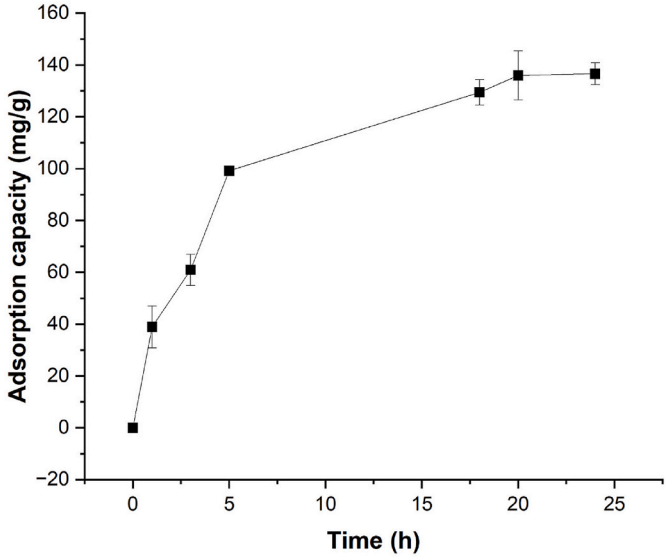

Fig. 6. Optimization of contact time on caffeine adsorption with commercial activated carbon derived from minerals (Error bars represent the standard deviation (n = 3)).

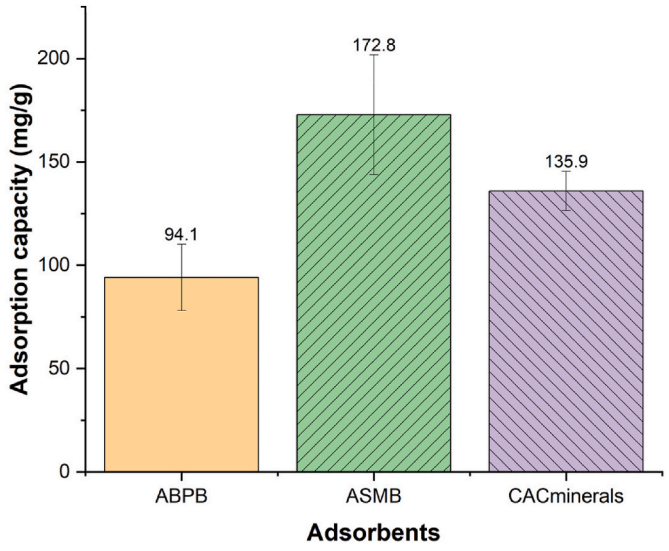

Fig. 7. Caffeine adsorption capacity measured for the adsorbents (ABPB: activated birchwood pellet biochar; ASMB: activated standard miscanthus biochar; $CAC_{minerals}$: commercial activated carbon derived from minerals; Error bars represent the standard deviation (n = 3)).

differences in caffeine adsorption capacities among the tested materials, with ABPB reaching 94 mg g^{-1}, while ASMB demonstrated a significantly higher capacity of 173 mg g^{-1}. The superior adsorption performance of ASMB can be attributed to its unique physical and chemical characteristics. Although ASMB possesses a lower SSA (398 m^2 g^{-1}) compared to ABPB (437 m^2 g^{-1}) and $CAC_{minerals}$ (585 m^2 g^{-1}), it still exhibited the highest adsorption capacity. This suggests that factors beyond surface area, such as pore structure, size distribution, and surface chemistry, play a critical role in adsorption efficiency. Elemental analysis further supports this observation, showing that ASMB has a lower carbon content (41.7%) compared to ABPB and $CAC_{minerals}$, along with a hydrogen content of 0.2%. An inferior carbon content indicates a higher presence of other elements or functional groups, which may influence its adsorption properties. In contrast, the relatively higher carbon content in ABPB and $CAC_{minerals}$ suggests a more carbon-rich

composition. Although hydrogen content across all adsorbents was low, its presence contributes to hydrogen bonding potential, with ASMB exhibiting a slightly greater capacity for such interactions than ABPB and $CAC_{minerals}$ due to its marginally higher hydrogen content.

The FTIR spectra of ABPB, ASMB, and $CAC_{minerals}$ indicated the presence of hydroxyl (-OH), carboxyl (-COOH), and aromatic functional groups, all of which facilitate interactions with caffeine molecules. Hydroxyl groups contribute to hydrogen bonding, enhancing adsorption efficiency, while carboxyl groups – being polar – enable electrostatic interactions and hydrogen bonding with caffeine. Additionally, the aromatic structures present on the adsorbent participate in π-π interactions with the aromatic rings of caffeine, further boosting adsorption performance. Specifically, FTIR analysis of ABPB showed pronounced aromatic C=C stretching, suggesting high aromaticity, which enhances π-π interactions with caffeine. ASMB, on the other hand, exhibited strong C-O stretching peaks, indicating the presence of oxygen-rich functional groups capable of forming strong hydrogen bonds with caffeine. These functional groups collectively enhance adsorption efficiency by providing multiple interaction sites, thereby increasing caffeine removal from aqueous solutions. These findings suggest that ASMB is a highly promising adsorbent for this application due to its superior adsorption capacity and favorable surface chemistry.

The initial pH value of a solution is crucial in adsorption processes, as it influences the physical and chemical properties of the adsorbent surface and the composition of adsorbate species in solution [39]. Biochar's amphoteric nature dictates its surface charge, which varies based on the solution pH and its point of zero charge (pH_{pzc}). Fig. 8 illustrates the variation of adsorption capacity with pH observed in the batch tests. Although only three representative pH values (2, 7, and 11) were examined in this study, these conditions provide a general assessment of adsorption performance under acidic, neutral, and alkaline environments. The maximum adsorption capacity values recorded were 97 mg g^{-1} for ABPB, 176 mg g^{-1} for ASMB, and 172 mg g^{-1} for $CAC_{minerals}$. Even though caffeine has a pKa of 10.4 [25], its charge state remains relatively neutral across a wide pH range because it lacks ionizable protons. As a result, electrostatic interactions between caffeine and biochar are negligible. The low pH dependence suggests that caffeine adsorption onto biochar is primarily driven by alternative interactions, including pore filling with π-π interactions, hydrogen bonding, van der Waals forces, and n-π interactions [2,9,36]. Given caffeine's molecular structure, these mechanisms likely dominate its adsorption onto biochar.

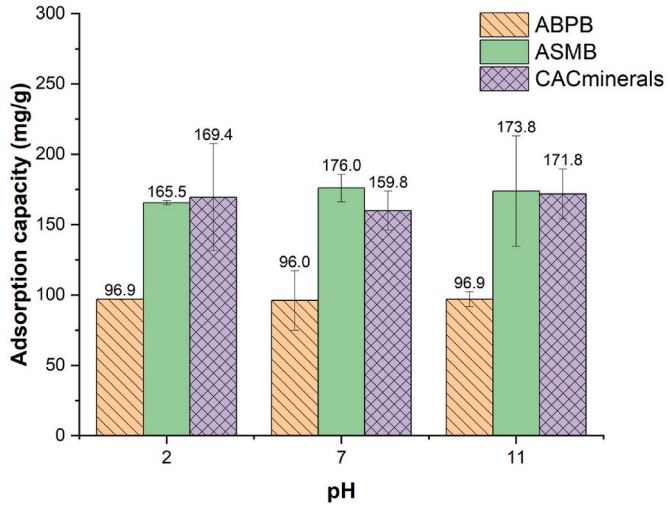

Fig. 8. Effect of pH on the adsorption of caffeine on the adsorbents (ABPB: activated birchwood pellet biochar; ASMB: activated standard miscanthus biochar; $CAC_{minerals}$: commercial activated carbon derived from minerals; Error bars represent the standard deviation (n = 3)).

A comparison with previously reported caffeine adsorption studies provides context for the adsorption performance observed in this work. CO_2-activated macrophyte-derived biochar exhibited a maximum adsorption capacity of approximately 118 mg g^{-1}, with adsorption governed primarily by π-π interactions and hydrogen bonding [4]. Biochars produced from fique bagasse showed lower capacities (~81 mg g^{-1}), yet similarly demonstrated pH-independent adsorption behavior dominated by non-electrostatic interactions [9]. Egusi-shell biochar pyrolyzed at 800 °C achieved an adsorption capacity of 121 mg g^{-1}, attributed to enhanced porosity and increased aromatic surface structures facilitating π-π and n-π interactions [2]. In contrast, pine-needle-derived biochars prepared at high temperatures exhibited substantially lower adsorption capacities (9–12 mg g^{-1}), which were linked to limited pore development and less favorable surface chemistry [46]. Compared with these studies, the adsorption capacities obtained in the present work (97–176 mg g^{-1}) fall within the upper range of values reported for biochar-based adsorbents. This comparison highlights the strong affinity of ABPB, ASMB, and $CAC_{minerals}$ for caffeine and reinforces that pore structure and aromatic surface chemistry – rather than electrostatic interactions – are the dominant factors governing caffeine adsorption onto biochar.

3.3. Desorption

3.3.1. Solvent desorption

Desorption efficiency varied significantly among the solvents (Fig. 9). Methanol and ethanol exhibited the highest efficiency, particularly for ASMB, which achieved 78% desorption with ethanol and 62% with methanol. $CAC_{minerals}$ showed 62% efficiency with methanol and 53% with ethanol, while ABPB displayed moderate desorption at 38% (in methanol) and 37% (in ethanol). 0.1M H_2SO_4, 0.1M NaOH, and DI water exhibited significantly lower desorption efficiency, all below 27% across all adsorbents. The superior performance of methanol and ethanol can be attributed to their high polarity, which facilitates strong interactions with caffeine, disrupting adsorption forces [47,48]. Their hydrogen bonding capabilities further enhance desorption by interacting with caffeine's functional groups [49]. Methanol's lower viscosity and smaller molecular size also aid penetration into the adsorbent pores, enhancing desorption. However, ethanol demonstrated comparable

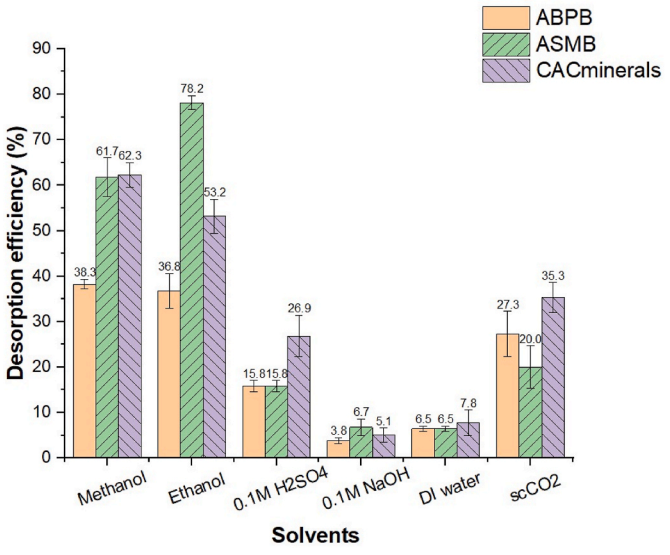

Fig. 9. Caffeine Desorption Efficiency from Various Adsorbents Using Different Solvents (ABPB: activated birchwood pellet biochar; ASMB: activated standard miscanthus biochar; $CAC_{minerals}$: commercial activated carbon derived from minerals; $scCO_2$: Supercritical Carbon Dioxide; Error bars represent the standard deviation (n = 3)).

efficiency, suggesting it as a viable alternative. In contrast, 0.1M H_2SO_4, 0.1M NaOH, and DI water showed low desorption efficiency due to weaker interactions with caffeine and the limited solubility of organic compounds in these solvents. These findings underscore the importance of solvent selection in optimizing desorption efficiency. While methanol is often favored for its solvent properties, ethanol provides a comparable alternative.

The desorption behavior observed in this study is consistent with previous reports on solvent-assisted regeneration of caffeine-loaded adsorbents. Dos Santos Lins et al. [50] demonstrated that methanol enabled more effective regeneration of MgAl-LDH/biochar composites compared with NaCl solutions, which was attributed to the stronger affinity of caffeine for polar organic solvents. Similarly, Lekene et al. [2] reported that ethanol and methanol were the most effective eluents for regenerating biochar-based adsorbents, whereas acidic, basic, and saline solutions exhibited limited regeneration performance. Although these studies primarily evaluated regeneration efficiency through adsorption-desorption cycles rather than directly quantifying caffeine desorption, their results consistently highlight the superiority of polar organic solvents. This trend aligns well with the present study, in which ethanol and methanol achieved the highest desorption efficiencies across all adsorbents, underscoring the critical role of solvent polarity in disrupting caffeine-adsorbent interactions.

3.3.2. *Supercritical CO_2 desorption*

Caffeine desorption efficiencies in $scCO_2$ were 27% for ABPB, 20% for ASMB, and 35% for $CAC_{minerals}$ (Fig. 9). The differences in desorption efficiency can be attributed to surface chemistry, CO_2-philicity, and the presence of inorganic components in the adsorbents. ASMB exhibited the lowest desorption efficiency, likely due to its higher oxygen-containing functional groups, which make the surface more polar and less CO_2-philic. Since supercritical CO_2 is a nonpolar solvent, it interacts less effectively with ASMB, leading to inefficient caffeine removal. Additionally, ASMB's higher ash content suggests a greater presence of minerals, which may have introduced stronger adsorption sites for caffeine, further hindering desorption.

In contrast, ABPB and $CAC_{minerals}$ demonstrated higher desorption efficiencies, likely due to their higher carbon content and lower ash content, which make them more compatible with $scCO_2$. Their surface chemistry and pore structure facilitate better interactions between $scCO_2$ and caffeine, promoting more effective desorption.

These findings highlight the critical role of adsorbent composition and CO_2-philicity in $scCO_2$ desorption efficiency. Further optimization, such as modifying surface chemistry or introducing co-solvents, may improve caffeine removal under supercritical conditions.

From a practical perspective, factors such as economic cost, energy consumption, and environmental impact should also be considered when selecting regeneration strategies for large-scale applications. Solvent-based desorption using organic solvents such as methanol or ethanol can achieve higher regeneration efficiencies but may require solvent recovery and generate secondary waste streams. In contrast, supercritical CO_2 regeneration offers the advantage of using CO_2 as a relatively clean solvent that can be easily separated after the process. However, the operation of supercritical CO_2 systems typically requires specialized equipment and higher energy input due to elevated pressure conditions. Therefore, while the present study focuses primarily on regeneration efficiency and technical feasibility, further techno-economic and environmental assessments will be necessary to evaluate the practical applicability of these regeneration approaches.

4. Conclusions

This study systematically evaluated caffeine adsorption and subsequent adsorbent regeneration using two CO_2-activated biochars derived from birchwood pellets and miscanthus, with a commercial mineral-derived activated carbon as a benchmark. By integrating adsorption performance and desorption behavior within a single experimental framework, this work provides new insights into the role of adsorbent physicochemical properties in both caffeine removal and adsorbent recovery.

Among the tested materials, the activated miscanthus biochar (ASMB) exhibited the highest caffeine adsorption capacity, reaching up to 176 mg g^{-1}, despite having a lower specific surface area (398.3 m^2 g^{-1}) than both activated birchwood pellet biochar (ABPB, 437.3 m^2 g^{-1}) and commercial activated carbon (585.0 m^2 g^{-1}). This result highlights that caffeine adsorption is governed not solely by surface area, but also by pore structure and surface chemistry. In particular, the higher abundance of oxygen-containing functional groups in ASMB enhanced hydrogen bonding interactions with caffeine, while aromatic domains contributed to π-π interactions and pore-filling mechanisms. The weak dependence of adsorption capacity on solution pH further confirmed that non-electrostatic interactions dominate caffeine adsorption onto carbonaceous adsorbents.

Regeneration of caffeine-loaded adsorbents was strongly influenced by the desorption method and the chemical nature of the adsorbents. Solvent-based desorption demonstrated that polar organic solvents, particularly ethanol and methanol, achieved the highest desorption efficiencies across all materials, reaching up to 78% for ASMB. In contrast, acidic, alkaline, and aqueous media were considerably less effective (<27%), underscoring the importance of solvent polarity and hydrogen bonding capacity in disrupting caffeine-adsorbent interactions. Supercritical CO_2 ($scCO_2$) desorption enabled solvent-free regeneration but exhibited lower desorption efficiencies compared to organic solvents, ranging from 20% to 35% depending on the adsorbent. Carbon-rich adsorbents with lower oxygen content, such as ABPB and commercial activated carbon, showed greater compatibility with $scCO_2$, whereas the more polar and ash-rich ASMB exhibited limited desorption. These findings emphasize the crucial role of surface polarity, ash content, and CO_2-philicity in determining $scCO_2$ desorption performance.

Overall, this study demonstrates that activated biochars derived from waste biomass can outperform commercial activated carbon in caffeine adsorption while offering viable regeneration pathways. The direct comparison between solvent-based and $scCO_2$ desorption provides a practical basis for selecting regeneration strategies tailored to adsorbent composition and sustainability objectives. While organic solvents currently offer higher regeneration efficiencies, $scCO_2$ represents a promising green alternative that could be further optimized through surface modification or the use of co-solvents. These results contribute to the development of sustainable adsorption-regeneration systems for the removal of emerging contaminants from water.

Declaration of generative AI and AI-assisted technologies in the manuscript preparation process

During the preparation of this manuscript, the authors used AI tools to assist with language editing and improving clarity and readability of the text. After using this tool, the authors critically reviewed and edited the content as needed and take full responsibility for the content of the published article.

CRediT authorship contribution statement

Heejin Lee: Data curation, Formal analysis, Investigation, Writing – original draft. **Silvia Fiore:** Conceptualization, Supervision, Visualization, Writing – review & editing. **Franco Berruti:** Conceptualization, Funding acquisition, Methodology, Resources, Supervision, Writing – review & editing.

Acknowledgements

The authors are grateful to the several industry partners and to the Natural Sciences and Engineering Research Council of Canada for

financial support of this research through the Industrial Research Chair program.

Data availability

The data that has been used is confidential.

References

[1] I. Anastopoulos, A. Katsouromalli, I. Pashalidis, Oxidized biochar obtained from pine needles as a novel adsorbent to remove caffeine from aqueous solutions, J. Mol. Liq. 304 (2020) 112661, https://doi.org/10.1016/j.molliq.2020.112661.

[2] R.B.N. Lekene, T.M.M. Ntep, M.N.A. Fetzer, T. Strothmann, J.N. Nsami, C. Janiak, The efficient removal of ibuprofen, caffeine, and bisphenol A using engineered egusi seed shells biochar: adsorption kinetics, equilibrium, thermodynamics, and mechanism, Environ. Sci. Pollut. Res. 30 (2023) 100095–100113, https://doi.org/10.1007/s11356-023-29377-w.

[3] S. Keerthanan, S.M. Rajapaksha, L. Trakal, M. Vithanage, Caffeine removal by Gliricidia sepium biochar: influence of pyrolysis temperature and physicochemical properties, Environ. Res. 189 (2020) 109865, https://doi.org/10.1016/j.envres.2020.109865.

[4] H.G. Zanella, L. Spessato, G.K.P. Lopes, J.T.C. Yokoyama, M.C. Silva, P.S.C. Souza, A. Ronix, A.L. Cazetta, V.C. Almeida, Caffeine adsorption on activated biochar derived from macrophytes (Eichornia crassipes), J. Mol. Liq. 340 (2021) 117206, https://doi.org/10.1016/j.molliq.2021.117206.

[5] V. Shukla, D. Panchal, O. Prakash, P. Mondal, I. Hiwrale, R.S. Dhodapkar, S. Pal, Magnetically engineered sulfurized peat-based activated carbon for remediation of emerging pharmaceutical contaminants, Bioresour. Technol. 369 (2023) 128399, https://doi.org/10.1016/j.biortech.2022.128399.

[6] H. Lee, S. Fiore, F. Berruti, Adsorption of methyl orange and methylene blue on activated biocarbon derived from birchwood pellets, Biomass Bioenergy 191 (2024) 107446, https://doi.org/10.1016/j.biombioe.2024.107446.

[7] G. Loebsack, K.K.-C. Yeung, F. Berruti, N.B. Klinghoffer, Impact of biochar physical properties on adsorption mechanisms for removal of aromatic aqueous contaminants in water, Biomass Bioenergy 194 (2025) 107617, https://doi.org/10.1016/j.biombioe.2025.107617.

[8] D. Dos Santos, W. Moreira, T. De Araújo, M. Bernardo, I. Fonseca, I. Ostroski, M. A. De Barros, Removal of emerging contaminants from water by using carbon materials derived from tingui shells, Separations 11 (2024) 215, https://doi.org/10.3390/separations11070215.

[9] Y.M. Correa-Navarro, J.C. Moreno-Piraján, L. Giraldo, Processing of fique bagasse waste into modified biochars for adsorption of caffeine and sodium diclofenac, Braz. J. Chem. Eng. 39 (2022) 933–948, https://doi.org/10.1007/s43153-021-00191-6.

[10] H. Lee, Adsorption and Desorption of Emerging Pollutants with Engineered Biochar Adsorbents, Western University, 2024.

[11] P. Cheng, Z. Li, Y. Zheng, Q. Meng, Y. Yu, Y. Jin, X. Gao, X. Guo, L. Jia, Study on the regulation of performance and Hg0 removal mechanism of MIL-101(Fe)-derived carbon materials, Sep. Purif. Technol. 379 (2025) 134939, https://doi.org/10.1016/j.seppur.2025.134939.

[12] Z. Shirani, V. Carrasco-Navarro, J. Sorvari, Effective adsorption of pharmaceuticals by plant based-activated biochar, water, Air. Soil Pollut. 236 (2025) 872, https://doi.org/10.1007/s11270-025-08526-6.

[13] S.I. Mustapha, K.B. Muritala, A.M. Afolabi, M.H. Alhaji, T.L. Adewoye, F. A. Aderibigbe, Phenol removal from pharmaceutical effluent using silver doped magnetite biochar: adsorption efficiency and kinetic studies, Chem. Eng. Commun. 213 (2026) 21–41, https://doi.org/10.1080/00986445.2025.2519294.

[14] D.F. Dos Santos, W.M. Moreira, T.P. De Araújo, M.M.S. Bernardo, I.M. De Figueiredo Ligeiro Da Fonseca, I.C. Ostroski, M.A.S.D. De Barros, Competitive adsorption of acetaminophen and caffeine onto activated tingui biochar: characterization, modeling, and mechanisms, Environ. Sci. Pollut. Res. 31 (2023) 53611–53628, https://doi.org/10.1007/s11356-023-31024-3.

[15] B. Belhamdi, H. Laksaci, C. Belabed, Z. Merzougui, S. Boudiaf, R. Tir, M. Trari, Synthesis of highly porous activated carbon derived from kernel oil treatment by-products of Argania spinosa as a recyclable adsorbent for amoxicillin removal from real wastewater, Biomass Convers. Biorefinery (2021), https://doi.org/10.1007/s13399-021-01380-6.

[16] V. Choudhary, L. Philip, Sustainability assessment of acid-modified biochar as adsorbent for the removal of pharmaceuticals and personal care products from secondary treated wastewater, J. Environ. Chem. Eng. 10 (2022) 107592, https://doi.org/10.1016/j.jece.2022.107592.

[17] M.N. Nasruddin, M.R. Fahmi, C.Z.A. Abidin, T.S. Yen, Regeneration of spent activated carbon from wastewater treatment plant application, J. Phys., Conf. Ser. 1116 (2018) 032022, https://doi.org/10.1088/1742-6596/1116/3/032022.

[18] D.H.D.S. Santos, Y. Xiao, N. Chaukura, J.M. Hill, R. Selvasembian, C.L.P.S. Zanta, L. Meili, Regeneration of dye-saturated activated carbon through advanced oxidative processes: a review, Heliyon 8 (2022) e10205, https://doi.org/10.1016/j.heliyon.2022.e10205.

[19] D.N. Mengesha, M.W. Abebe, R. Appiah-Ntiamoah, H. Kim, Ground coffee waste-derived carbon for adsorptive removal of caffeine: effect of surface chemistry and porous structure, Sci. Total Environ. 818 (2022) 151669, https://doi.org/10.1016/j.scitotenv.2021.151669.

[20] U. Salgın, İ. Alomari, N. Soyer, S. Salgın, Adsorption of bisphenol A onto β-Cyclodextrin–Based nanosponges and innovative supercritical green regeneration of the sustainable adsorbent, Polymers 17 (2025) 856, https://doi.org/10.3390/polym17070856.

[21] M. Sanchez-Montero, J. Pelaz, N. Martin-Sanchez, C. Izquierdo, F. Salvador, Supercritical regeneration of an activated carbon fiber exhausted with phenol, Appl. Sci. 8 (2018) 81, https://doi.org/10.3390/app8010081.

[22] W. Kim, J. Kim, S. Oh, Supercritical carbon dioxide extraction of caffeine from Korean green tea, Separ. Sci. Technol. 42 (2007) 3229–3242, https://doi.org/10.1080/01496390701513008.

[23] Y. Hiraga, C. Yoshida, K. Aoki, M. Watanabe, Efficient decaffeination of green coffee beans using pressure swing supercritical CO2 extraction, Innov. Food Sci. Emerg. Technol. 104 (2025) 104154, https://doi.org/10.1016/j.ifset.2025.104154.

[24] J. Shao, J. Zhang, X. Zhang, Y. Feng, H. Zhang, S. Zhang, H. Chen, Enhance SO2 adsorption performance of biochar modified by CO2 activation and amine impregnation, Fuel 224 (2018) 138–146, https://doi.org/10.1016/j.fuel.2018.03.064.

[25] I.J.M. Duarte, T.M.I.D.O. Lima, A.M.D.M. França, H.L.D.B. Buarque, R.F. Do Nascimento, Adsorption of caffeine using steel wastes, Environ. Sci. Pollut. Res. 29 (2022) 79977–79994, https://doi.org/10.1007/s11356-022-19582-4.

[26] L. Lin, Y. Zhang, H. Zhang, F. Lu, Adsorption and solvent desorption behavior of ion-exchanged modified Y zeolites for sulfur removal and for fuel cell applications, J. Colloid Interface Sci. 360 (2011) 753–759, https://doi.org/10.1016/j.jcis.2011.04.075.

[27] J.-Y. Yoon, J.E. Kim, H.J. Song, K.B. Oh, J.W. Jo, Y.-H. Yang, S.H. Lee, G. Kang, H. J. Kim, Y.-K. Choi, Assessment of adsorptive behaviors and properties of grape pomace-derived biochar as adsorbent for removal of cymoxanil pesticide, Environ. Technol. Innov. 21 (2021) 101242, https://doi.org/10.1016/j.eti.2020.101242.

[28] D. Kołodyńska, J. Krukowska, P. Thomas, Comparison of sorption and desorption studies of heavy metal ions from biochar and commercial active carbon, Chem. Eng. J. 307 (2017) 353–363, https://doi.org/10.1016/j.cej.2016.08.088.

[29] S. Jiang, L. Yan, R. Wang, G. Li, P. Rao, M. Ju, L. Jian, X. Guo, L. Che, Recyclable nitrogen-doped biochar via low-temperature pyrolysis for enhanced lead(II) removal, Chemosphere 286 (2022) 131666, https://doi.org/10.1016/j.chemosphere.2021.131666.

[30] A. Herath, C.A. Layne, F. Perez, E.B. Hassan, C.U. Pittman, T.E. Mlsna, KOH-activated high surface area douglas fir biochar for adsorbing aqueous Cr(VI), Pb(II) and Cd(II), Chemosphere 269 (2021) 128409, https://doi.org/10.1016/j.chemosphere.2020.128409.

[31] J. Chen, C. Tang, X. Li, J. Sun, Y. Liu, W. Huang, A. Wang, Y. Lu, Preparation and modification of rape straw biochar and its adsorption characteristics for methylene blue in water, Water 14 (2022) 3761, https://doi.org/10.3390/w14223761.

[32] K. Wystalska, A. Kwarciak-Kozłowska, Utilization of digestate from agricultural and food waste for the production of biochar used to remove methylene blue, Sustainability 15 (2023) 14723, https://doi.org/10.3390/su152014723.

[33] L. Puri, Y. Hu, G. Naterer, Critical review of the role of ash content and composition in biomass pyrolysis, Front. Fuels 2 (2024) 1378361, https://doi.org/10.3389/ffuel.2024.1378361.

[34] W. Huang, J. Chen, J. Zhang, Adsorption characteristics of methylene blue by biochar prepared using sheep, rabbit and pig manure, Environ. Sci. Pollut. Res. 25 (2018) 29256–29266, https://doi.org/10.1007/s11356-018-2906-1.

[35] P. Boakye, H.N. Tran, D.S. Lee, S.H. Woo, Effect of water washing pretreatment on property and adsorption capacity of macroalgae-derived biochar, J. Environ. Manag. 233 (2019) 165–174, https://doi.org/10.1016/j.jenvman.2018.12.031.

[36] G. Loebsack, K.K.-C. Yeung, F. Berruti, N.B. Klinghoffer, Adsorption of organic pollutants from wastewater using biochar: a mechanistic study on competitive adsorption behavior, Water Environ. Res. 97 (2025) e70164, https://doi.org/10.1002/wer.70164.

[37] A. Bano, M.K. Aziz, R. Mishra, H. Dave, B. Prasad, M. Kumari, D. Dubey, L. Meili, M.P. Shah, K.S. Prasad, Response surface methodology–based optimisation of adsorption of diclofenac and treatment of pharmaceutical effluent using combined coagulation-adsorption onto nFe2O3 decorated water chestnut shells biochar, Environ. Sci. Pollut. Res. 31 (2024) 55317–55335, https://doi.org/10.1007/s11356-024-34799-1.

[38] C. Zhao, J. Ma, Z. Li, H. Xia, H. Liu, Y. Yang, Highly enhanced adsorption performance of tetracycline antibiotics on KOH-activated biochar derived from reed plants, RSC Adv. 10 (2020) 5066–5076, https://doi.org/10.1039/C9RA09208K.

[39] B. Zhang, Y. Wu, L. Cha, Removal of methyl orange dye using activated biochar derived from pomelo peel wastes: performance, isotherm, and kinetic studies, J. Dispersion Sci. Technol. 41 (2020) 125–136, https://doi.org/10.1080/01932691.2018.1561298.

[40] J. Lykiema, K.S.W. Sing, J. Haber, M. Kerker, E. Wolfram, J.H. Block, N. V. Churaev, D.H. Everett, R.S. Hansen, R.A.W. Haul, J.W. Hightower, R.J. Hunter, Prepared for Publication by the Subcommittee on Reporting Gas Adsorption Data Consisting of K. S. W. SING (UK, Chairman); D. H. EVERETT (UK); R. A. W. HAUL (FRG); L. MOSCOU (Netherlands); R. A. PIEROTTI (USA); J. ROUQUEROL (France); T. SIEMIENIEWSKA (Poland), 1984.

[41] N.X. Loc, P.T.T. Tuyen, L.C. Mai, D.T.M. Phuong, Chitosan-modified biochar and unmodified biochar for methyl Orange: Adsorption characteristics and mechanism exploration, Toxics 10 (2022) 500, https://doi.org/10.3390/toxics10090500.

[42] S. Chen, M. Zhou, H.-F. Wang, T. Wang, X.-S. Wang, H.-B. Hou, B.-Y. Song, Adsorption of reactive brilliant red X-3B in aqueous solutions on clay–biochar composites from bagasse and natural attapulgite, Water 10 (2018) 703, https://doi.org/10.3390/w10060703.

[43] H. Nath, A. Saikia, P.J. Goutam, B.K. Saikia, N. Saikia, Removal of methylene blue from water using okra (Abelmoschus esculentus L.) mucilage modified biochar, Bioresour. Technol. Rep. 14 (2021) 100689, https://doi.org/10.1016/j.biteb.2021.100689.

[44] M. Masuku, J.F. Nure, H.I. Atagana, N. Hlongwa, T.T.I. Nkambule, Pinecone biochar for the adsorption of chromium (VI) from wastewater: Kinetics, thermodynamics, and adsorbent regeneration, Environ. Res. 258 (2024) 119423, https://doi.org/10.1016/j.envres.2024.119423.

[45] H. Zeghioud, L. Fryda, A. Mahieu, R. Visser, A. Kane, Potential of flax shives and beech wood-derived biochar in methylene blue and carbamazepine removal from aqueous solutions, Materials 15 (2022) 2824, https://doi.org/10.3390/ma15082824.

[46] O. Oginni, K. Singh, Effect of carbonization temperature on fuel and caffeine adsorption characteristics of white pine and Norway spruce needle derived biochars, Ind. Crops Prod. 162 (2021) 113261, https://doi.org/10.1016/j.indcrop.2021.113261.

[47] B. Du, C. Chen, Y. Sun, M. Yang, M. Yu, B. Liu, X. Wang, J. Zhou, Efficient and controllable ultrasound-assisted depolymerization of organosolv lignin catalyzed to liquid fuels by MCM-41 supported phosphotungstic acid, RSC Adv. 10 (2020) 31479–31494, https://doi.org/10.1039/D0RA05069E.

[48] Y. Zhang, F. Jiang, D. Huang, S. Hou, H. Wang, M. Wang, Y. Chi, Z. Zhao, A facile route to magnetic mesoporous core–shell structured silicas containing covalently bound cyclodextrins for the removal of the antibiotic doxycycline from water, RSC Adv. 8 (2018) 31348–31357, https://doi.org/10.1039/C8RA05781H.

[49] D. Sanyal, P. Mathur, Advanced adsorbent mediated extraction techniques for the separation of antibiotics from food, biological, and environmental matrices, Separ. Purif. Rev. 51 (2022) 373–407, https://doi.org/10.1080/15422119.2021.1954950.

[50] P.V. Dos Santos Lins, D.C. Henrique, A.H. Ide, C.L. De Paiva E Silva Zanta, L. Meili, Evaluation of caffeine adsorption by MgAl-LDH/biochar composite, Environ. Sci. Pollut. Res. 26 (2019) 31804–31811, https://doi.org/10.1007/s11356-019-06288-3.